As-built building information modeling: joint effort of 3D reconstruction and semantic enrichment

Fan Xue
Assistant Professor, Dept. of Real Estate and Construction, The University of Hong Kong, China. ORCID: 0000-0003-2217-3693, e-mail: xuef@hku.hk

This is the pre-print of the following Chapter:

Xue, F. (2022). As-built building information modeling: joint effort of 3D reconstruction and semantic enrichment. In Lu W. & Anumba, C. (eds.) Research Companion to Building Information Modeling. Edward Elgar, in press.

The final version is available at: https://www.e-elgar.com/shop/gbp/research-companion-to-building-information-modeling-9781839105517.html . The use of this pre-print must follow the CC BY-NC ND License.

Abstract

As-built BIM represents a facility as actually constructed or as it currently exists. The information, such as actual geometry, current functions, and real topology, in as-built BIM is vital to construction research and smart city development. Two complementary classes of methods, i.e., digital 3D reconstruction and semantic enrichment, were applied, yet to consolidate, for as-built BIM creation in the literature. This paper presents a general framework that formulates the two classes as a joint effort. Two illustrative cases, one on outdoor rooftops and the other on indoor furniture, were employed to explain how the two streams of approaches can co-create as-built BIMs. Two future directions, i.e., digital twin building and blockchain BIM, are discussed. As a result, the semantically rich as-built BIM forges a shared construction information hub for smarter applications.

Keywords

As-built BIM; 3D reconstruction; semantic enrichment; digital twin; 3D point cloud

1. Introduction

A building information model (BIM), also known as building information modeling, is the digital representation of physical and functional characteristics of a facility, according to the definition by the National BIM Standard of United States (NIBS, 2015). BIM acts as a shared information resource and knowledge base regarding the facility. Based on the information and knowledge shared, construction stakeholders are thereby able to have a reliable basis for decisions making (NIBS, 2015).

Information is the keyword in BIM (Lu, Lai, & Tse, 2019). The as-built information is particularly vital to building research and smart city applications. Generally, there are two types of information (also known as semantics) contained in a BIM (Eastman, Teicholz, Sacks, & Liston, 2011; Belsky, Sacks, & Brilakis, 2016; Xue, Lu, & Chen, 2018).

1) Regarding an individual construction component, e.g.:
    a. Geometric information, such as size, position, shape and textures; and
    b. Non-geometric information, such as type, specifications of material, and meanings of functions.
2) Regarding relationships between components, such as dependency, topology, and joints.

A BIM can be "blind" and "deaf" if it does not reflect the real situations of a construction (Chen, Lu, Peng, Rowlinson, & Huang, 2015). Furthermore, some critical information, such as actual building geometries, current functions, and real topology of facilities, are only embodied in as-built BIMs (Xiong, Adan, Akinci, & Huber, 2013; Pătrăucean, et al., 2015). Semantically rich as-built BIMs can enable many value-added applications, including facility management, building retrofitting and renovation, energy consumption simulation, indoor positioning, and augmented reality (AR). Otherwise, the inevitable design changes, inadvertent deviations or errors, and renovation work make an 'as-designed' BIM inappropriate for various applications. Only by reenergizing a BIM with the as-built (or as-is) information of actual and current situations, one can update the as-designed BIM to as-built BIM to reflect and represent the real facility (Pătrăucean, et al., 2015).

However, the wide adoption of BIM in the architectural, engineering and construction (AECO) industry was very recent. Most constructions around the world do not have BIM representations; needless to say about the as-built information in BIM. In summary, there is a large gap between the need and the availability of as-built BIM for many existing constructions. An as-built BIM modeling is manually doable in a small scale, for example, in as-built modeling of one heritage building (Bruno, De Fino, & Fatiguso, 2018). Regarding the extreme number of buildings and irregular geometries in a larger context, e.g., a city, manual work is extremely tedious, time-consuming, and costly (Xue et al. 2020b). Researchers have thus endeavored to develop various automated (i.e., automatic or semi-automatic) as-built modeling approaches over the past decade (Xiong, Adan, Akinci, & Huber, 2013).

In as-built BIM creation, no matter manual or automated, there are two groups of methods, i.e., 3D reconstruction and semantic enrichment. The two groups must work together to update all the as-built information, i.e., geometric, non-geometric individual, and relational. For example, if the geometric model is not available, 3D reconstruction can create the as-built geometry from measurement data. Otherwise, if the 3D geometric model is ready to reuse,

e.g., from an as-designed BIM or reconstructed 3D model, semantic enrichment can update it with the latest information (Xue et al. 2019b).

This chapter aims to present a general framework of as-built BIM creation for BIM automation and applications in the construction industry. The next section summarizes related work. Section 3 describes the framework. Two cases, including one outdoor case of rooftop elements and the other of indoor furniture, are presented in Sections 4 and 5 to demonstrate how the 3D reconstruction and semantic enrichment work collaboratively. In addition, the recent evolving trend of as-built BIM to a digital twin is discussed and a conclusion is drawn.

2. Related Work

2.1 As-built BIM

Every construction has a lifecycle, also a learning cycle. Along the whole cycle, BIM, as the shared construction information hub, goes through as-required, as-designed, as-planned, as-built (or "as-is"), as-altered, and as-demolished versions (Xue, Lu, & Chen, 2018). The as-built BIM mainly covers the building, use, and maintenance phases. That is, as-built BIM is also the longest persistent version of BIM for a facility. The generation of such BIMs has therefore attracted the interest of practitioners and academics in the architecture, engineering, construction, and operations (AECO) industry, urban geology, robotics, and autonomous vehicle.

2.2 3D Reconstruction of Buildings

The geometric data sources of buildings are becoming accurate, detailed, diversified, and—perhaps most importantly—affordable. In tradition, taped-measured lengths, e.g., height, and depth, used to be the main forms of 3D geometry. The 2D imagery was also an important geometric data source (Ellenberg, Kontsos, Moon, & Bartoli, 2016). In recent one or two decades, more and more types of 3D surveying digital measurements have been adopted in the AECO industry. Examples are laser scanning by total station, photogrammetry (or structure from motion) by drones, RGBD images by depth camera, mobile scanning of simultaneous localization and mapping (SLAM) by AR smartphones and vehicles (Wang & Kim, 2019; Xu, et al., 2020).

Considerable progress has also been made in enhancing data preparations (e.g., point cloud registration), developing preprocessing algorithms, and exploring model generation methods (Hamledari, McCabe, & Davari, 2017; Sacks, et al., 2017).These efforts responded to the challenges in the geometric data sources. For example, point clouds and imagery primarily represent the surface geometry, which makes it difficult to reveal the volumetric components

and discover non-geometric semantics from the surfaces. In addition, point clouds and imagery are even limited in collecting all the surfaces—sometimes only one side with big and small holes—of a facility.

'Semantic segmentation' refers to a process of partitioning each pixel to a semantic label (Shamir, 2008), which has been successfully applied in object surfaces extraction and BIM components creation (Barazzetti, 2016; Babacan, Chen, & Sohn, 2017). There are four broad classifications of the segmentation-based 3D reconstruction methods: a priori rules, geometric shape descriptors, machine learning classifiers, and a composition of numerous BIM components. Employing the regularity of individual component is a priori rule for BIM object recognition, such as the prism boundary reconstruction of indoor space (Valero, Adán, & Cerrada, 2012). Performing the shape matching by extracting the characteristic geometric features as an explicit shape descriptor, such as the Laplace-Beltrami filtering (Wang, et al., 2018). The machine learning classifiers has also been applied in Babacan et al. (2017)'s research on convolutional neural network. Many studies have adopted a combination of multiple segmentation methods for multiple BIM components, such as Nguyen and Choi (2018) detached planar primitives before RANSAC fitting of cylindrical pipe systems. Notwithstanding that the reconstruction of simple shaped and regularly shaped objects has been successfully utilized through these semantic segmentation-based methods, there still exists disadvantages: substandard performance for complex shaped objects (e.g., furniture) (Wang, et al., 2018); reliance on a priori rules or labeled data set for models training; and failure to reuse online open BIM resources (Xue, Lu, & Chen, 2018).

To solve defects when dealing with complex-shaped objects, the segmentation-free methods are thus proposed. Xue et al. (2018) propositioned the semantic registration, a method based on nonlinear optimization for BIM reconstruction. Employing overall error minimization or similarity maximization between the reconstructed BIM and the measured data, a single BIM object will be reassembled into a complete model, thereby combining them with semantic information from reliable sources (Xue et al. 2019b). Thus far, semantic registration has been verified on 2D photos and 3D point clouds of indoor and outdoor scenes. Hidaka et al. (2018) developed another noteworthy method, in which the similar areas of template CAD model were first adaptively located, and then the iterative closest point (ICP) algorithm was employed to finely register the CAD templates. Besides, the mechanical, electrical and plumbing (MEP) systems from clashes can be reorganized through simulated annealing from Hsua and Wua (2019)'s outcomes. Although the abovementioned first three weaknesses of semantic segmentation have been addressed by segmentation-free methods, it still presents two limitations, i.e., low efficiency from unnecessary re-exploration of the problem search space and the proneness to input errors Xue et al. (2018; 2019b) and Hidaka et al. (2018).

2.3 Semantic Enrichment to Buildings

Semantic enrichment is a way of automatic or semiautomatic adding of meaningful information to an existing BIM (or 3D building) model, instead of creating a new model from scratches (Jardim-Goncalves, Sarraipa, Agostinho, & Panetto, 2011; Belsky, Sacks, & Brilakis, 2016). Instead of creating a new BIM from scratches, one can apply semantic enrichment to use and reuse the existing 3D models of a facility. One main reason is that the geometry of a facility is usually rigid, as a whole or in most parts, for reusing. Another reason lies in the multi-disciplinary collaboration in obtaining and understanding the as-built conditions of a facility. Semantic enrichment, as a way of inter-disciplinary interoperability of information, showed strengths in other domains, such as database management systems, manufacturing, and semantic web (Lacasta, Nogueras-Iso, Falquet, Teller, & Zarazaga-Soria, 2013; Liao, Lezoche, Panetto, & Boudjlida, 2016). Furthermore, cities and buildings are evolving over time. A BIM deems to be updated from time to time, otherwise it may become "blind" and "deaf." Apart from the moving city objects, the facilities which seem to have steady geometries require their non-geometric information such as functions and property valuations to be updated from time to time (Chen, Lu, Peng, Rowlinson, & Huang, 2015).

Semantic enrichment usually combines and correlates the measurement data and a priori semantic model. Yet, some studies relied more on the measurement data. For example, Koppula et al. (2011) predicted the semantic labels of indoor points based on edge potentials. Lin et al. (2013) classified the LiDAR point clouds into patches of geometric primitives, then reconstructed connected graphs of patches for building model enrichment such as the hole filling and surface enclosure. Yang et al. (2020) extracted the 3D dimensions from CAD drawings for semi-automatic BIM enrichment. Deep learning models that predict semantic labels from 3D point clouds, such as types of building components in Chen et al. (2019) and Pierdicca et al. (2020), also became popular recently.

More research applied and adapted a priori semantic models to describe the measurement data, like design patterns, rules, and domain knowledge. For instance, Kim et al. (2013) registered as-built measurement point cloud to an as-planned BIM to update the schedule. Liu and Wu (2016) presented a rule-based method to reconstruct historical buildings with different architectural styles. Chen et al. (2018) applied a fundamental regularization rule to rooftop elements from noisy LiDAR data. Other examples included the topological rule processing in the SeeBIM system (Sacks, et al., 2017) and a knowledge-based system for resolving design clashes in BIMs (Hsu, Chang, Chen, & Wu, 2020).

3. A General Framework of Creating As-built BIM

Figure 1 shows a general framework of creating and applying an as-built BIM. As shown in Figure 1, the conceptual model includes five interrelated components, namely, (1) The target facility, (2) Baseline model, (3) Sources of new semantics, (4) Semantic enrichment method, and (5) Enriched model. For a given facility, semantic enrichment is the process that extracts new semantics from the new semantics sources and adds them to the baseline BIM or CIM so that the updated model has a richer digital representation of the facility.

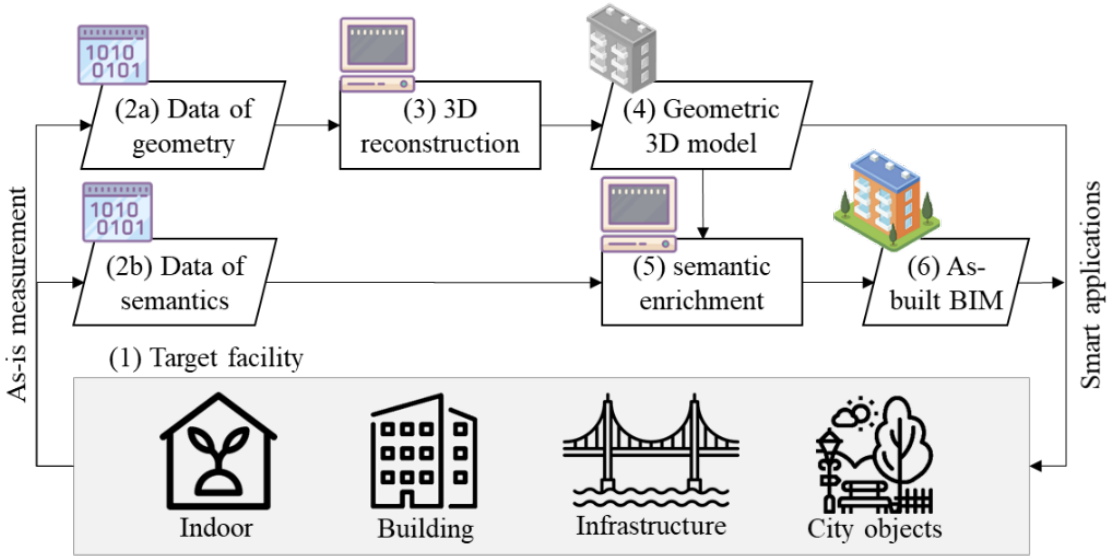

Figure 1. A general framework of as-built BIM creation

The target facility is the primary subject of an as-built BIM. The facility also plays the roles of the ultimate information source and value-added application sink. The types of facilities may include: (i) indoor objects and systems like furniture and space network, (ii) buildings, (iii) civil infrastructures, and (iv) other city objects.

The data sources in Figure 1 consist of two types, i.e., data of geometry and semantics data. Data of as-is geometry, which serves the purpose of 3D reconstruction mainly, can be collected, registered, integrated, and resampled from laser scanning, photogrammetry, or tape measurements (Baltsavias, 1999; Jung, et al., 2014). In contrast, semantics data enables semantic enrichment to non-geometric and relational information to the as-built BIM, while the data sources include non-geometric measurements, such as cement temperature from infrared sensors and laser reflection from LiDAR, and existing models from designers and manufacturers (Xue, Lu, Tan, & Chen, 2019c). Sometimes, the two data sources are intertwined. For example, the 3D coordinate (x, y, z) in a LiDAR point cloud is the geometric

data, while the laser reflectance denoting how much percentage of laser beams returned is a column of data of semantics.

The 3D reconstruction methods can create 3D surfaces and volumetric BIM components for a facility based on the geometric data sets. Digital 3D construction, focusing on creating the geometric form from 2D plans or point data, has a deep root in Computer-aided Design (CAD) and Computer Vision and Pattern Recognition (CV/PR) since the 1980s. The result is as a geometric 3D building model, sometimes a volumetric BIM. The geometric model or BIM can enable several smart applications, e.g., solar power potential, fresh air ventilation, and sky view simulations.

Semantic enrichment, in comparison, originated in database management systems (DBMS) and emphasizes the non-geometric functions and relational attributes in BIM. For example, the accuracy of building energy model and urban heat island simulations can be improved with the building surface materials predicted from laser reflectance in the LiDAR point clouds and colors in 2D photographs. Furthermore, 3D reconstruction processes and semantic enrichment are expected to run periodically to maintain the as-is geometric conditions and current functions in an as-built BIM.

4 An Outdoor Case of Rooftop Elements

4.1 A Case at the University of Hong Kong

The study area, in this case, was a squared area around the University of Hong Kong (HKU) Main Campus, about 0.3 km^2 in the Central Western District, Hong Kong. As shown in Figure 2, the LiDAR data was collected by the Civil Engineering and Development Department (CEDD) of the Hong Kong SAR Government (CEDD, 2015). The intensity in the LiDAR data was measured by an airborne Optech 3100 LidAR sensor. The point density was about 4.0 points per m^2. The study area consisted of various urban landscapes, including high-density urban blocks.

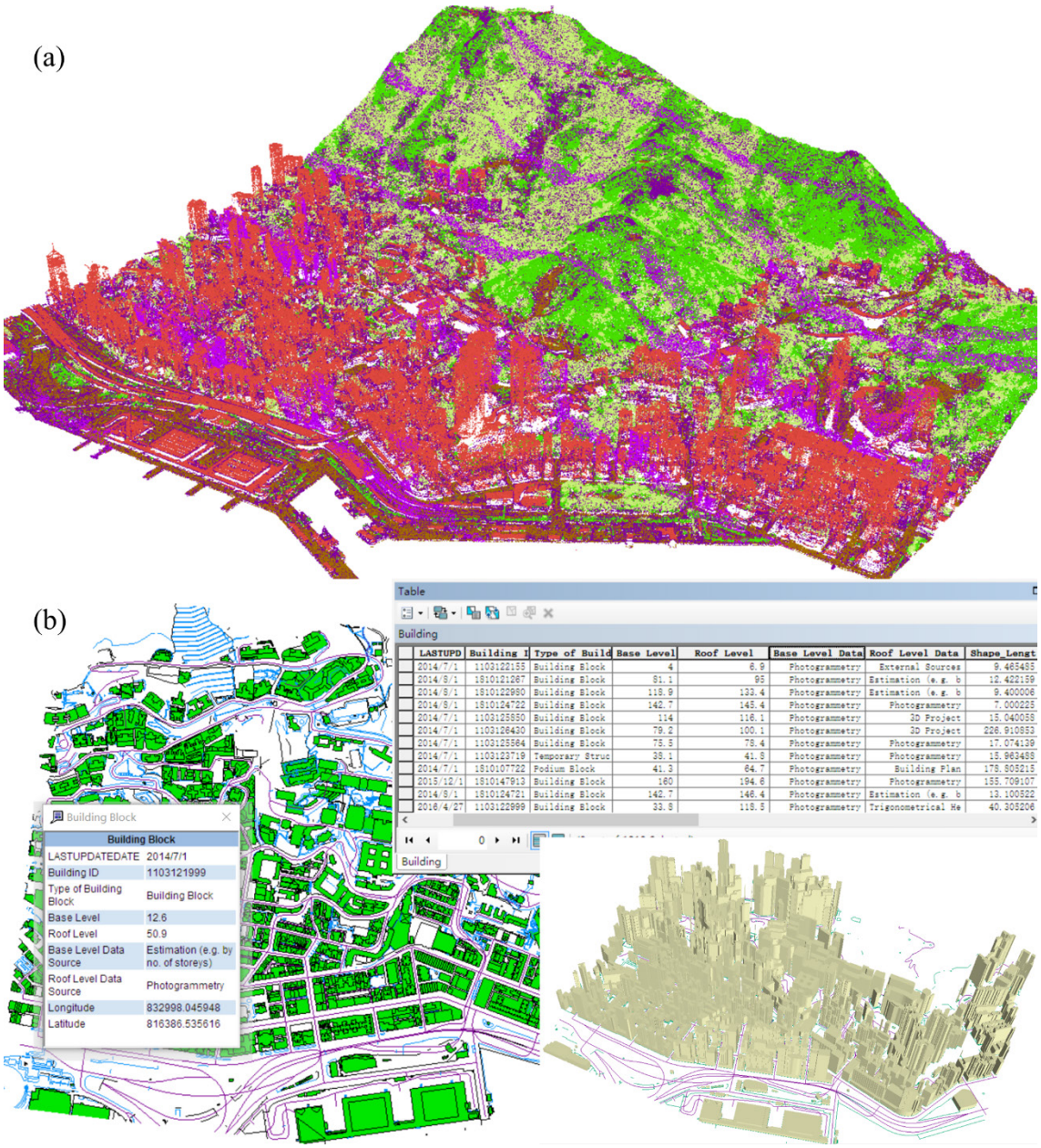

Figure 2. The study area. (a) The CEDD (2015) LiDAR data, (b) topographic map and LoD1 (2.5D) objects (Source: authors; Chen et al. (2018))

Both 3D reconstruction and semantic enrichment tests were conducted to the rooftop elements in the test case. Roofs usually constitute 20~25% urban surfaces in typical metropolises (Rose, Akbari, & Taha, 2003). Rooftop albedo that measures how much solar radiation is reflected (other than absorbed) by roof coatings leads to a negative radiative forcing. At a worldwide level, high-albedo roofs can offset billions of tons of CO_2 emissions as well as save billions of dollars of energy bills every year (Akbari, Menon, & Rosenfeld, 2009). Therefore, some governments, such as the California Energy Commission (2005), have required all new or retrofitted roofs to be white or reflective.

Apart from the LiDAR point cloud, an official topographic map was also used in the tests. The map, as shown in Figure 2b, was a 1:1000 Geodatabase (GDB) format digital map from the Lands Department (LD) of HKSAR. The 2D city objects were described in the Hong Kong 1980 Grid system (EPSG:2326), which mean all the x, y, z, values were in meter. The map contains 2D city objects such as buildings, land cover, and transportation. The 2D buildings in Figure 2b were highlighted. The building footprints and heights were used in this case.

4.2 3D Reconstruction

The 3D reconstruction is completed by an integrated approach named multi-Source recTification of gEometric Primitives (mSTEP), presented in Chen et al. (2018). The mSTEP consists of four phases in as-built modeling. The first phase is 2.5D building polygons creation was visualized in ESRI ArcScene, as shown in Figure 2b. The geometric data source was the building footprints in the official topographic map. The results were Level of Details 1 (LoD1) building blocks in terms of the CityGML standard.

The second step aims to extract considerable (e.g., with > 1 m diameter) rooftop elements from the rooftop point clouds. First, the point cloud of each building was segmented. The boundary for segmentation was extended from the building footprint, because some buildings have slightly larger roof area than its foot. An iterated RANSAC (Schnabel, Wahl, & Klein, 2007) was adopted for detecting geometric primitives from LiDAR point cloud of the building rooftops. It is decided to set the minimum number of support points of RANSAC to 10 (i.e., element top area no less than 2.5 m^2), maximum distance to primitive to 0.02 m, and sampling resolution to 1.0.

The third step detects the guiding directions (lines) from the building footprints. The perpendicular and parallel lines of the long edges in a footprint can indicate the major axes in the building design. Regular-shaped footprints and irregular-shaped ones can drive the guiding directions. As a result, the 3D reconstruction took advantage of both as-built measurement of LiDAR point clouds and as-designed building footprints. Figure 3 shows how the mSTEP method could achieve the goal. The mSTEP was tested on a personal notebook with 2.6GHz Quad-core CPU, 16 GB RAM, and a 64-bit Microsoft Windows 10 operating system. First LoD2 as-built BIM is developed by aligning the rooftop elements to the guiding directions. Particularly, two object rectification rules were employed, as shown in Figure 3ab. In tests, the maximum normal deviations of α and β were set to 25°.

Figure 3f shows eight examples of reconstructed building models involving various architectural features, for examples, an Edwardian Baroque-style building (ID: 11**374) including a central clock tower and corner turrets on the Main Campus of HKU; a high-rise residential building (ID: 11**486) with a pyramidal roof, surrounded by several irregular roof objects; a food wholesale market (ID: 11**535) with some parallel strips as well as box-shaped air conditioners on the roof; and a convex-shaped roofed building (ID: 11**845). It can be further noticed that no manual post-modification is required for those reconstructed models. It can be seen that the models reaching LoD2 retain more details than simple "boxes", and achieve acceptable criteria.

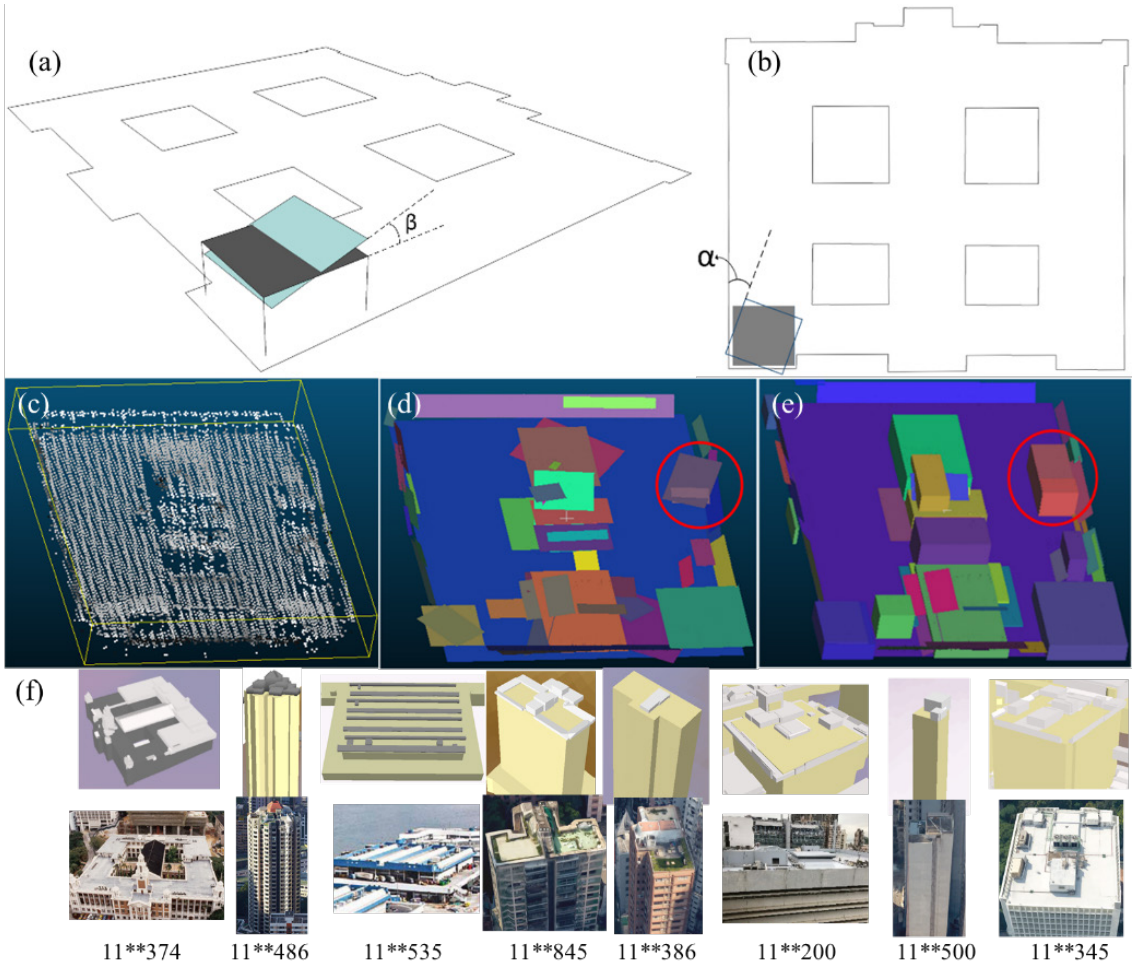

Figure 3. Reconstruction and rectification of rooftop objects according to the guiding lines. (a) First vertical adjustment rule; (b) second horizontal adjustment rule; (c) LiDAR point clouds; (d) geometric primitives; (e) output; (f) Examples of the reconstructed LoD2 BIMs and the ground truth photographs. (Source: authors; Chen et al., (2018))

Table 1 compares mSTEP and Javanmardi et al.'s (2015) method using three metrics: (i) root-mean-squared error (RMSE) between the associated points and the BIM, (ii) percentage of segmented points (associated with as-built BIM), and (iii) computational time. Both methods reconstructed accurate geometry, in terms of RMSE, for segmenting the point clouds; while mSTEP was more accurate (average RMSE = 0.085 m). Furthermore, mSTEP segmented more points (81.3% on average) to support as-built BIM creation. However, Javanmardi et al.'s (2015) method was faster. The comparison results show that the 3D reconstruction was successful and competitive against other methods for building rooftops.

Table 1. Comparison of mSTEP's results (best values in bold)

No.	*Number of points*	*mSTEP*			*Javanmardi et al.* (2015)†		
		Time (s)	*Segmented (%)*#	*RMSE (m)**	*Time (s)*	*Segmented (%)*#	*RMSE (m)**
1	270	0.03	75.2	0.114	0.02	63.1	0.119
2	372	0.03	77.7	0.048	0.01	58.7	0.157
3	620	0.40	87.6	0.065	0.02	84.7	0.098
4	2,491	0.16	48.6	0.196	0.05	31.6	0.199
5	2,682	0.09	90.0	0.057	0.03	60.2	0.049
6	7,212	0.23	91.1	0.067	0.04	26.4	0.067
7	8,987	0.26	85.1	0.065	0.09	18.8	0.097
8	24,878	2.23	86.3	0.068	0.13	66.2	0.163
9	29,506	0.47	90.1	0.088	0.21	71.1	0.230
Average		0.48	**81.3**	**0.085**	**0.07**	53.4	0.131

†: The paprameter β of Javanmardi et al. (2015)'s method was set to 0.5m as the average point distance;
#: Percentage of points that are segmented to support the detection of geometric primitives.
*: Root mean square error of the distances of segmented points to their corresponding primitives.

4.3 Semantic Enrichment

4.3.1 Rooftop Albedos

Two data-driven applications of semantic enrichment were tested on the basis of the LoD2 as-built BIMs. To monitor rooftop albedos and utilize them in simulations, Xue et al. (2019c) created a semantic as-built city information model (CIM) of rooftop albedos in the target area. The whole modeling process was straightforward. First, the geometric models of 1,087 blocks of buildings and 1,288 rooftop elements on top of them were created using the method in Chen et al. (2018). Then, the values of albedos were estimated using a linear model of the near-infrared laser reflectance, according to the validation in Levinson et al. (2014). The enriched rooftop albedos are vital to various urban sustainability topics such as heat island, local climate, green roof, and urban morphology (Santamouris, 2014; Stewart, Oke, & Krayenhoff, 2014; Baniassadi, Heusinger, & Sailor, 2018). The enriched as-built model converted into GeoJSON formats and visualized on a web 3D library OSMBuildings (version

3.0.1, https://github.com/OSMBuildings/OSMBuildings). Figure 4a shows the visualized albedo models of the study area.

Beside of the albedo, Xue et al. (2019c) associated each rooftop model with the topographical map of Hong Kong (in HKGS1980 coordinate system) and *Open Street Map* (in WGS1984). As a result, more semantic properties can be enriched to the model of the building. Figure 4b shows the Knowles Building, HKU, in which the offices of the authors reside, in the web visualization system. Apart from the geometric dimensions, one can read the more properties from the mouse tooltip: Name, building IDs in the topographic map and *Open Street Map*, roof albedo (0.351), type of building, storeys (including the level of basements). In comparison to the model in Google Earth, as shown in Figure 4.c, all rooftop elements including the parapet walls, elevators' machine rooms, water tank, and cooling towers, except for one circled. Since the albedo is not available in Google Earth, and the GeoJSON is an open GIS format, the albedo models presented in this paper can facilitate more in sustainability study.

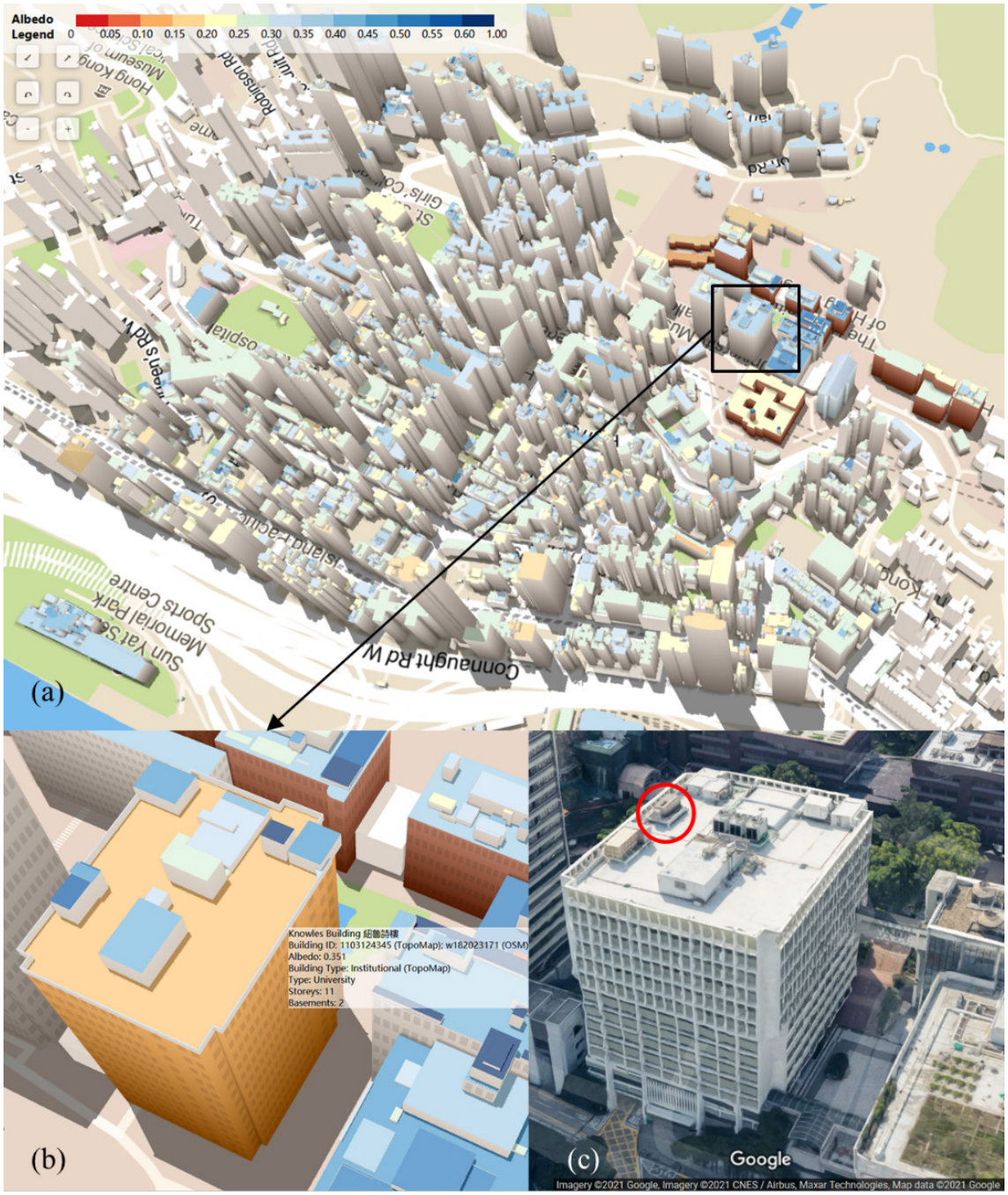

Figure 4. Results of rooftop albedo enrichment. (a) LiDAR-based albedo; (b) Example of an enriched LoD2 BIM; (c) the referential 3D model (Source: Google Earth).

4.3.2 Green Rooftop Element Prediction Enrichment

The other semantic enrichment test was conducted in Tan et al. (2019) on the green roof elements prediction. In a small area of 55,000 m^2 in the target campus, there existed a few green roofs. There were two types of green roofs, i.e., turf and potted. In addition, we found the laser reflectance might have correlations with the green roof. Therefore, the classification of green roof elements from the remainder of reconstructed geometric primitives can be another task of semantic enrichment for this study.

In the pilot case, green roof elements are identified into two types: turf, where vegetation covering the entire surface of the roof; potted area, where plants live in pots or containers. Table 5a shows the excerpt of the data table of the pilot case for classification and enrichment, including average reflectance in percentage, the top area of each element in square meter, height in meter. The computational analyses were conducted on a Windows 10 work area PC. The decision tree was trained by the *rpart* bundle (ver. 4.1), which is freely accessible on the R stage (ver. 3.4). The boundaries of the choice tree are: "min part = 2," "max profundity = 5," and "min container = 1." Figure 5c shows the green rooftop components detection prepared by the decision tree, which utilized under 0.01s to get the last precise outcomes. Figure 5d shows the comparison of predicted green rooftops and aerial view of the 3D model on Google Earth. The screen capture of Google Earth shows genuine green rooftop components. The green areas, found primarily on top of three buildings, are highly correlated to the predicted green rooftop components. The semantic enrichment of the green rooftop makes our model semantically rich in terms of computer readable greenery.

(a)

	A	B	C	D	E
1	en	albedo_pct	area_m2	height	
2	Non-green	54.49779736	123.5969	2.473763	
3	Non-green	53.63681592	66.17113	2.386444	
4	Non-green	36.72314815	400.519	3.532402	
5	Non-green	34.59036145	58.62441	3.517059	
6	Non-green	50.82051282	12.508	2.835854	
7	Non-green	29.5	5.046435	0.797977	
8	Non-green	30.5	9.466119	0.716205	
9	Non-green	33.47058824	29.10006	0.627361	
10	Non-green	28.09090909	5.260042	0.721675	
11	potted	35.09589041	74.02478	0.346179	
12	turf	54.93457944	61.92282	-0.34778	
13	turf	53.72502523	529.2725	-0.33987	
14	turf	50.36821705	74.39653	-0.39377	
15	Non-green	71.95522388	32.26995	1.062436	
16	Non-green	70.2862069	223.3756	0.984464	

(b)

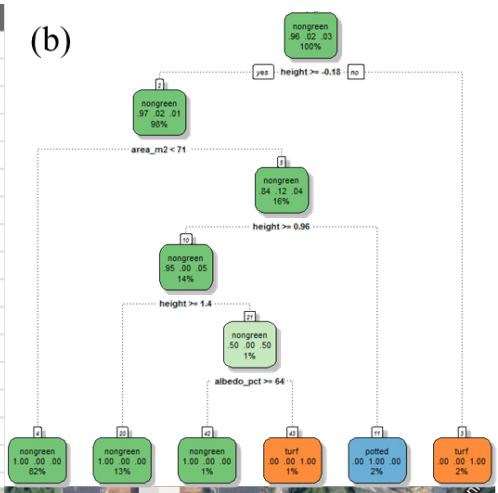

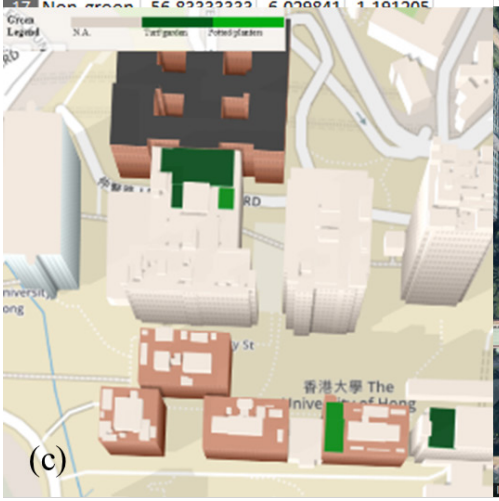

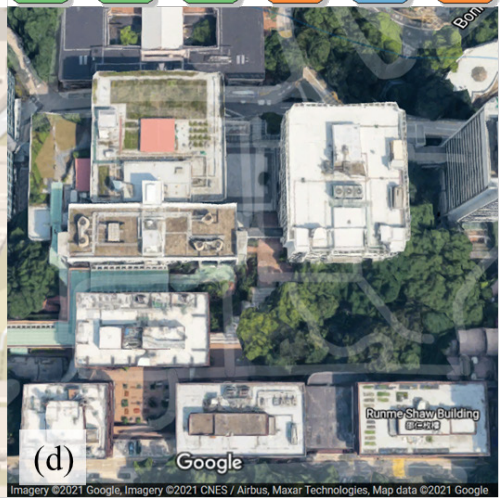

Figure 5. A small area of buildings with green roofs. (a) Excerpt of the training data; (b) the learned decision tree; (c) prediction results (dark = truf, light = potted); (d) Aerial view (Source: Google Earth).

5. An indoor case of furniture

5.1 A case at the Stanford University

We selected the largest indoor instance in the Stanford 2D-3D-S dataset (Armeni, Sax, Zamir, & Savarese, 2017) to demonstrate the as-built modeling. The "Area_2 Auditorium_2" instance is the largest lecture hall room in a university building at the Stanford University.

Furthermore, it is known that indoor point clouds are more challenging for as-built modeling in general. First, the regular large planar objects such as floor and walls were removed because they are relatively easy to reconstruct. The removal took advantage of the given labels in the dataset. As a result, a noisy 'scene' cloud of 293 theater chairs remained as shown in Figure 6.a. The cloud $S = \{ p_1, p_2, \ldots, p_n \} \subset \mathbb{R}^3$ of n = 1,879,282 points. As shown in the right bottom corner in Figure 6.a, some parts were considerably noisy, incomplete, and cluttered. The study area was 14.80m x 14.87m. From the general design principles, we assumed every chair has 4 degrees of freedoms (DoFs) including the 3D location t_x, t_y, t_z, and the heading direction r_z, while the rotations around x and y axes were not allowed. Figure 6c visualizes the expected fitness landscape, which was very jagged over the x-y plane. It should be noted that the z and r_z were set as the optimal values. The spikes in Figure 6c are the optimal transformation parameters $[t_x, t_y]^T$ (or modes). Figure 6d is the vertical projection, in which we can see the patterns are the x-y positions of the chairs.

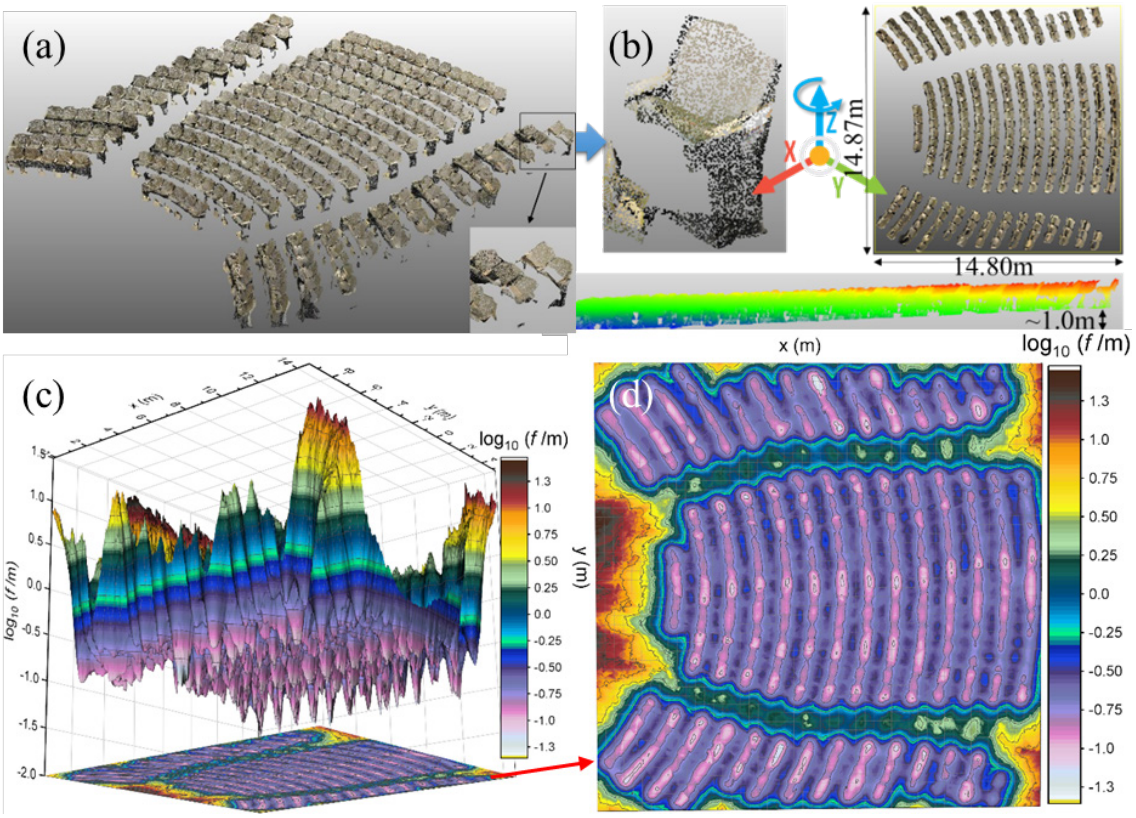

Figure 6. The indoor study case. (a) A noisy scene cloud S of 293 chairs (1,879,282 points); (b) the 4 degrees of freedom and boundary; (c) surface chart; (d) Contour chart in (a) (Source: authors; Xue et al. (2019a))

5.2 3D Reconstructions using Unimodal and Multimodal Algorithms

The 3D reconstruction was formulated as a semantic registration approach by Xue et al. (2019b). Furthermore, two classes of optimization algorithms, i.e., a 'unimodal' algorithm CAM-ES and a multimodal algorithm NMMSO, were tested in parallel. As required by the semantic registration, an open BIM component 'Theater chair' was downloaded from a 3D model sharing website *3DWarehouse.com*. The surfaces of the component were sampled into

a cloud $\mathcal{C}$ of 1,802,939 points using an in-house developed Autodesk Revit plugin developed in Xue et al. (2019b).

Given the scene cloud S (n points) and a 'component' cloud $\mathcal{C} = \{ p_1, p_2, \ldots, p_m \} \subset \mathbb{R}^3$ of m points, the task of 3D reconstruction for as-built BIM creation is equivalent to an optimization problem that finds all the instances of $\mathcal{C}$ in S in the semantic registration paradigm (Xue et al. 2019b):

$$
\begin{aligned}
\textbf{arg min}\ \ & f(x) = RMSE(\mathcal{C}(x), S) = \left[\frac{1}{m}\Sigma_{p\in(x)} \parallel p - N(p,S) \parallel^2\right]^{1/2} \\
\textbf{s.t.}\ & \mathcal{C}(x) = \{T_x(p) | p \in \mathcal{C}\}, \\
& T_x(p) = \mathrm{R}\,(p) + [t_x,\ t_y,\ t_z]^T \\
& \mathrm{R} = \begin{bmatrix} \cos r_z & -\sin r_z & 0 \\ \sin r_z & \cos r_z & 0 \\ 0 & 0 & 1 \end{bmatrix}, \\
& x = [t_x,\ t_y,\ t_z]^T \in R^6 \\
& [t_x, \quad t_y, \quad t_z]^T \in boundingbox(C) \\
& r_z \in [0, 2\pi) \\
& f(x) \leq \varepsilon = 0.25 diag\mathcal{C} \approx 0.01 diagC
\end{aligned}
\qquad (1)
$$

Where *parent* is a function that returns the "parent" component that $\mathcal{C}(x)$ attaches to, *boundingbox* indicates the 3D bounding box of the scene cloud S (see Figure 6b), $diag_{\mathcal{C}}$ stands for the diagonal length of $\mathcal{C}$, and $diag_C$ is the diagonal length of C. Also, the regular layout of concentric circles of the chairs is in line with architectural acoustic input to theatre designs (Mehta, Johnson, & Rocafort, 1999).

Usually an optimal transformation parameters x^* yields $f(x^*) = f_{\min}$ (e.g., 0). However, regarding the possibility of instrumental, environmental, and calibration errors for the point cloud, as well as heterogeneous point density, geometric accuracy, occlusion, and clutters in the as-built measurement data, we relaxed the optimality condition to a satisfactory condition:

$$
X* = \{ x* \mid f(x*) \leq f\min + \varepsilon \}, \qquad (2)
$$

where x^* indicates *one* satisfactory solution (mode) to Eq. (1), X^* is the set of satisfactory solutions, and ε denotes a small error tolerance.

Figure 7a shows the results of a unimodal optimization algorithm named covariance matrix adaptation with evolution strategy (CMA-ES) to the solving of Eq. (1). The "unimodality"

means the algorithm returns one instance of chair each time. The as-built BIM in Figure 7a consisted of 288 chairs, saved as a 1.83 MB Revit file. Figures 10.7b shows the false negatives (undetected) and false positives (wrong location or rotation) of chairs in the generated as-built BIM from the top view. Figure 7c shows the results of a multimodal optimization algorithm named niching migratory multi-swarm optimizer (NMMSO). The "multimodality" stands for returning many, if not all, instances of chairs from one run. NMMSO took 414.5s to discover 300 solutions to Eq. (1) in the incremental build phase through the greedy processing (see Figure 2a). In the second stage, COBIMG-Revit was adopted and used CMA-ES to fine-tune the 300 chairs in BIM in 512.1s.

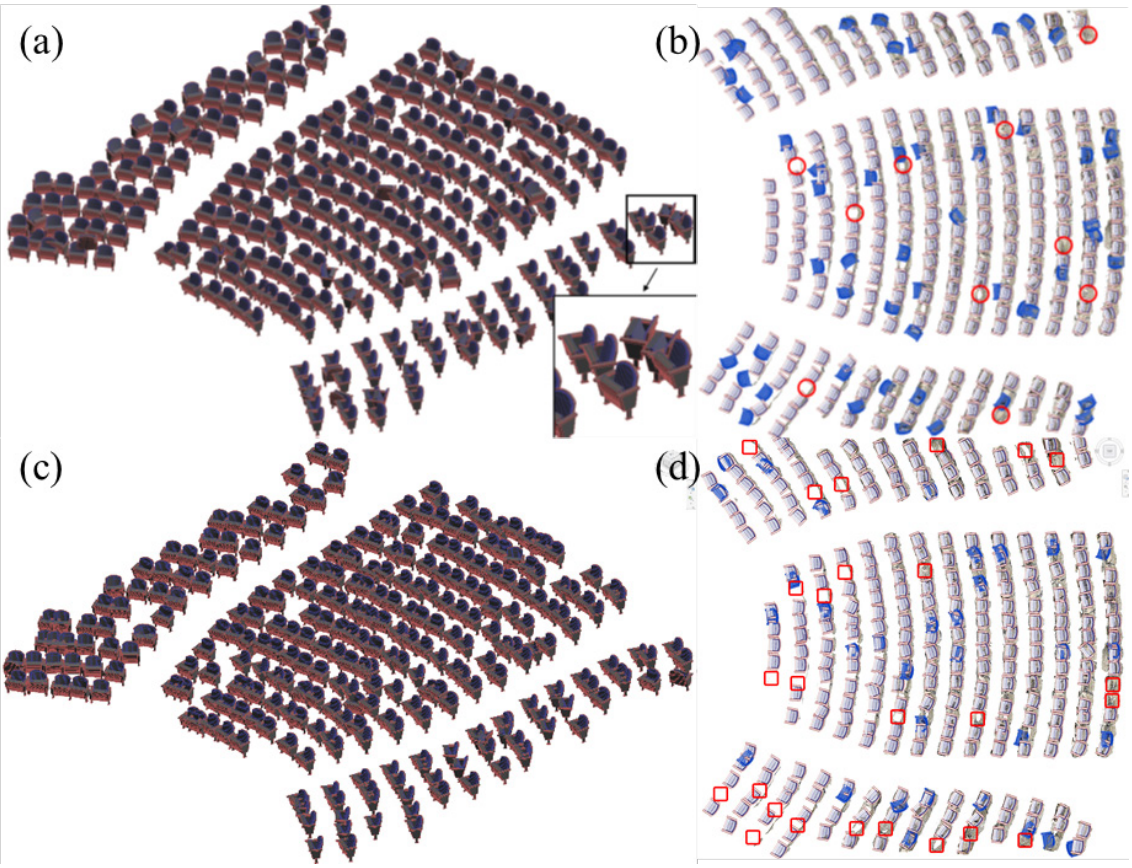

Figure 7. Results of 3D reconstructions. (a) As-built BIM of 288 chairs automatically reconstructed in 1434.2s by CMA-ES; (b) top view of 236 true positive chairs (wired frames), 52 false positives (dark), and 10 false negatives (circles); (c) as-built BIM of 300 chairs in 926.6s by NMMSO; (d) top view of 267 true positive chairs (wired frames), 33 false positive (dark), and 26 false negative (boxes). (Source: authors; Xue et al. (2019a))

The confusion matrix of the chairs in the output BIM was listed in Table 3. The accuracy metrics for the unimodal algorithm CMA-ES were thus:

$$\begin{aligned} precision &= \frac{\text{true positive}}{\text{true positive} + \text{false positive}} = \frac{236}{288} = 81.9\%, \\ recall \quad &= \frac{\text{true positive}}{\text{true positive} + \text{false negative}} = \frac{236}{288} = 80.5\ \%, \\ F_1 &= 2\, precision \times recall(precision + recall) = 81.2\%. \end{aligned} \tag{3}$$

Meanwhile, all three metrics of the multimodal algorithm NMMSO were about 10% higher than those by the unimodal optimization CMA-ES:

$$\begin{aligned} precision &= \frac{\text{true positive}}{\text{true positive + false positive}} = \frac{267}{300} = 89.0\%, \\ recall &= \frac{\text{true positive}}{\text{true positive + false negative}} = \frac{267}{300} = 91.1\%, \\ F_1 &= 2\, precision \times recall \,/\, (precision + recall) = 90.1\%. \end{aligned} \tag{4}$$

Table 3. A confusion matrix of the generated chairs in the generated

Evaluation	CMA-ES		NMMSO	
	Chairs	Not a chair	Chairs	Not a chair
Positive position and rotation	236	10	267	26
Positive position but negative rotation (error > 45°)	16	-	-	-
Negative position (error > 25cm*)	36	-	33	-
Subtotal	288	10	300	26

*: 25cm is a quarter of the diagonal of the target chair

5.3 Semantic Enrichment

The semantic enrichment, in this case, was a more model-driven procedure. As a lecture hall, the seats arrangement was set to the pattern of concentric circles for an optimal acoustic design (Mehta, Johnson, & Rocafort, 1999). Then, 14 clusters of seating rows were labeled manually in 223.7 s. An RMSE regression of arcs aims to find the patterns from the centroids of the chairs. The output equations for all chairs were in Equations (5). From Eq. (5), we can find the center of the stage center was at (–5.832 m, –2.091 m). In addition, the radius r increased perfectly linearly row by row ($R^2 = 0.9999$). Similarly, we got the regression Equation (6) for the z values of the chairs' centroids against x, y, and ρ in 0.06s. Eq. (6) shows the seat altitudes (z) were mainly in a linear relation with the row number. But, two more coefficients +0.005 and -0.003 suggested that the chairs had a 1:200 slope over the y-axis and a 1:330 slope over the x-axis. Or, it can be a small error in calibrating the Stanford dataset.

$$\begin{aligned} &(x + 5.832)^2 + (y + 2.091)^2 = r^2 \\ &\mathrm{r} = 0.913\,\rho + 7.387 \\ &\rho \in \{1,2,\ldots,14\} \\ &R^2 = 0.9999 \end{aligned} \tag{5}$$

$$\begin{aligned} &z = 0.418 + 0.061\,\rho - 0.003\,x + 0.005y \\ &\rho \in \{1,2,\ldots,14\} \\ &R^2 = 0.9673 \end{aligned} \tag{6}$$

The true pattern can be rebuilt from the symmetric regularization of the occupied arcs and isometric regularization of the angular distances between the chairs. First, the centers of groups of chairs were identified with local chairs as well the symmetric group of chairs, as shown in Figure 8a. Note that most of the missing chairs were compensated. In the isometric regularization, as shown in Figure 8b, the chairs in each extended cluster were first sorted by a clockwise order. The heading angles against the stage center (–5.832, –2.091) reordered the instances in 14 queues, then a maximum seat gap (or the minimum width of an aisle) at twice of the chair distance (2 × 55.26cm) segmented each queue into three groups. As a result, the 14 clusters of 289 chairs were grouped into 42 sets. The z values were aligned to Eq. (6), accordingly.

The semi-automatic regularization-based semantic enrichment (and 3D fine-tuning) processing took extra 228.6s after the 3D reconstruction. As shown in Figures 10.8c, a remarkable improvement was attained in the error distributions. The final as-built BIM achieved an accuracy at 99.3%, a recall at 98.0%, and an F_1 score at 98.6%, in terms of the chairs. The RMSE between the BIM visible surface and the input field cloud was 8.79cm. In terms of ground-truth values, the average distance error was 9.6cm and the average angular error was 3.8°.

The semantics of the concentric design pattern was enriched to the as-built BIM. The output was a 1.82 MB Autodesk Revit file. Figure 8e shows the screenshot of the properties of the first chair, with geometric information obtained from 3D reconstruction and semantic information from semantic enrichment. Some properties, such as e.g., "COBIMG_translation" and "COBIMG_rotation" indicate location, heading direction, and parent component. Furthermore, some properties such as "COBIMG_cluster" and "COBIMG_peer_left" note the semantics of the cluster, group, sequence, and the "neighbor" components of each chair.

Table 4 compares the results of the as-built BIM creation in this section. The metrics include the RMSE between the measurement 3D points and the as-built BIM, time cost, 3D position error of chair centroids, angular error of r_z, precision, recall, and F_1 score. The accuracy of the automatic 3D reconstruction by NMMSO was about 10% higher than CMA-ES, with 35% time saved versus CMA-ES. Furthermore, the as-built BIM with regularization-based semantic enrichment had an even better 99.3% precision and 90% recall, while the time was still less than CMA-ES. Besides, one can find an interesting collision between the global RMSE error and local BIM object (chair) based error metrics. The CMA-ES had the best RMSE but the lowest precision and recall of chairs.

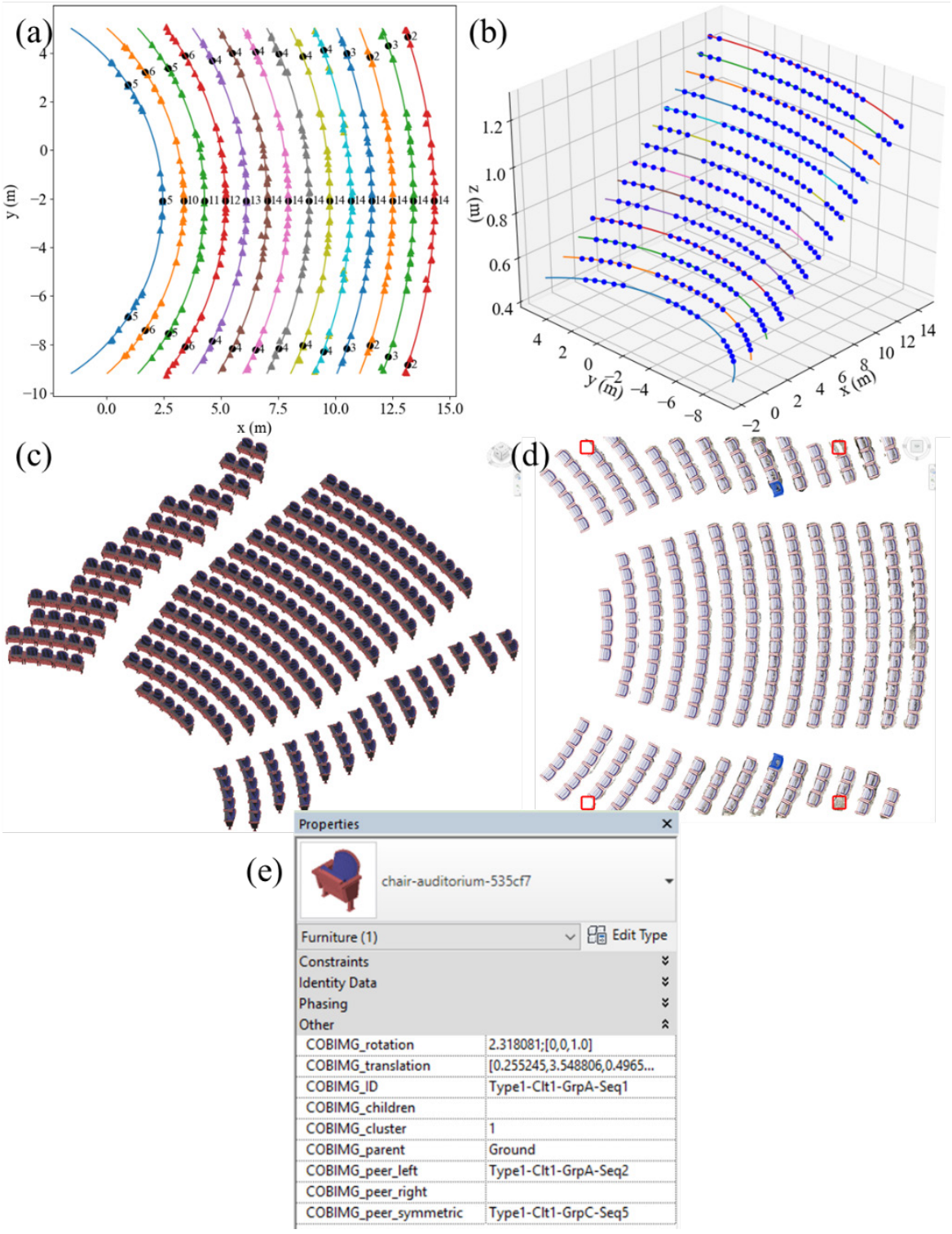

Figure 8. Results of semantic enrichment of the as-built BIM. (a) Symmetric and isometric regularizations based on Eqs. (5) and (6); (b) 3D centroids of 289 regularized chair positions using the detected repetition equations; (c) the regularized and enriched model; (d) top view of 287 true positive chairs, 2 false positive (dark), and 4 false negative (boxes); (e) enriched semantic information. (Source: authors; Xue et al. (2019a))

Table 4. Comparison of different algorithms on BIM chair detection, where the best value in each row is in bold

Evaluation (unit)	*CMA-ES*	*NMMSO*	*NMMSO + semantic enrichment*
RMSE (cm)	**8.10**	10.38	8.97
Computational time (s)	1,434.2	**926.6**	1,155.0
Number of chairs	288	300	**289**
Distance error (cm, mean ± stdev.)	15.2 ± 7.7	13.7 ± 6.5	**9.6 ± 3.5**
Angular error (°, mean ± stdev.)	17.6 ± 28.8	10.5 ± 15.0	**3.8 ± 3.3**
Precision (%)	81.9	89.0	**99.3**
Recall (%)	80.5	91.1	**98.0**
F_1 (%)	81.2	90.1	**98.6**

6 Toward Digital Twin and Blockchain BIM

There are, at least, two possible technological streams to push as-built BIM further. One is escalating the 'as-built' to a real-time virtual replica, i.e., digital twin. The other is extending the 'BIM' from isolated model files to an incremental process of changes and an interconnected chain of reliable information (Xue, Wu, & Lu, 2021).

A digital twin is a "virtual representation of a physical object or system across its lifecycle, using real-time data to enable understanding, learning, and reasoning," according to UK National Infrastructure Commission (2017). A digital twin with real-time data and information can monitor, simulate, and analyze complex systems. Examples of such systems include aircrafts, wind turbines, production shop floors, and building systems without close adjacency to the system physically. The value of digital twin lies in the monitored, simulated, and analytical results that can reveal emergent behaviors and mitigate unpredictable and undesirable consequences (Grieves & Vickers, 2017). By definition, a real-time updated as-built BIM is a digital twin, i.e., digital twin building. Apart from the 3D reconstruction and semantic enrichment approaches, a digital twin building requires real-time data collection and near-real-time processing. Data imperfections, such as heterogeneous point density, geometric accuracy, occlusion, and clutters, challenges as-built BIM creation and digital twinning (Barazzetti, 2016). However, an integration of 3D digital reconstruction and semantics, e.g., global patterns of repetitive furniture as shown in Sect. 5.2 and Xue et al.'s (2020b) cross-sections of unknown symmetric objects, can ease the problems of data imperfections for building and city objects designed in design principles. Thus, the framework of digital twinning is an updated version of that of as-built BIM creation, with real-time sensors, communication networks, and systematic and efficient model updating mechanisms.

Xue and Lu (2020a) pinpointed another future direction as differential BIM changes and blockchain BIM. A subsequent challenge after the digital twin building is the trackability and traceability of the historical BIMs and information. It is incredibly inefficient to derive independent and isolated BIM files hour after hour, day after day. Because most as-built BIM components remain unchanged, one needs to back up the changes to the as-built BIM only. In other words, the temporal redundancy of the unchanged as-built information in many copies of BIM files should be eliminated. Xue and Lu (2020a) presented a feasible semantic differential transaction (SDT) approach that detects the minimal BIM changes in the semantic hierarchy. Another challenge can be distributed as-built BIM changes from different stakeholders at different physical places. Thus, a blockchain BIM architecture maintained by a permissioned group can synchronize all the BIM changes to form the blockchain BIM.

7 Conclusion

As-built BIM reflects the actual and current situations of a facility. To fulfill smarter building and smarter city development, as-built BIM is a strategically important urban information infrastructure. Based on the work presented in the literature and the demands in the industry, this paper concludes a general framework for as-built BIM creation and application. Notably, the 3D reconstruction of geometry and semantic enrichment of non-geometric and relational information are complementary means in the presented framework.

Two demonstrative cases, one outdoor and the other indoor, are employed to explain the framework. Furthermore, one case shows how 3D measurement data is distilled for a 3D geometric model, while the other case shows how standard and open 3D BIM components are able to be utilized for as-built BIM creation. In the semantic enrichment to the outdoor case, the new semantic information, like albedos and green elements, was mainly driven by measurement data; in contrast, the new semantics was driven by knowledge as the concentric indoor design patterns.

Besides the various value-added applications of as-built BIM in the literature, two future research directions are advised. One is the digital twin technology that replicates and analyzes the target facility in real-time. A digital twin building is an upgrade version of as-built BIM that emphasizes the timely information synchronization and decision support. The other direction is minimal changes over the version history of an as-built BIM and the potential blockchain BIM which integrates all the as-required, as-designed, as-planned, as-built (or "as-is"), as-altered, and as-demolished BIMs of a facility throughout its lifecycle.

Acknowledgements

The work presented in this study was financially supported by grants from the Hong Kong Research Grant Council (Nos. 17201717 and 27200520).

References

Akbari, H., Menon, S., & Rosenfeld, A. (2009). Global cooling: increasing world-wide urban albedos to offset CO2. *Climatic change, 94*(3-4), 275-286. doi:10.1007/s10584-008-9515-9

Armeni, I., Sax, A., Zamir, A. R., & Savarese, S. (2017). Joint 2D-3D-Semantic Data for Indoor Scene Understanding. *ArXiv e-prints*, 1702.01105. Retrieved from https://arxiv.org/abs/1702.01105

Babacan, K., Chen, L., & Sohn, G. (2017). Semantic segmentation of indoor point clouds using Convolutional Neural Network. *ISPRS Annals of Photogrammetry, Remote Sensing and Spatial Information Sciences, IV-4*(W4), 101-108. doi:10.5194/isprs-annals-IV-4-W4-101-2017

Baltsavias, E. P. (1999). A comparison between photogrammetry and laser scanning. *ISPRS Journal of photogrammetry and Remote Sensing, 54*(2-3), 83-94. doi:10.1016/S0924-2716(99)00014-3

Baniassadi, A., Heusinger, J., & Sailor, D. J. (2018). Building energy savings potential of a hybrid roofing system involving high albedo, moisture retaining foam materials. *Energy and Buildings, 169*, 283-294. doi:10.1016/j.enbuild.2018.04.004

Barazzetti, L. (2016). Parametric as-built model generation of complex shapes from point clouds. *Advanced Engineering Informatics, 30*(3), 298-311. doi:10.1016/j.aei.2016.03.005

Belsky, M., Sacks, R., & Brilakis, I. (2016). Semantic enrichment for building information modeling. *Computer-Aided Civil and Infrastructure Engineering, 31*(4), 261-274.

Bruno, S., De Fino, M., & Fatiguso, F. (2018). Historic Building Information Modelling: performance assessment for diagnosis-aided information modelling and management. *Automation in Construction, 86*, 256-276. doi:10.1016/j.autcon.2017.11.009

California Energy Commission. (2005). *California Energy Commission Building Energy Efficiency Standards, For Residential and Nonresidential. Publication No. CEC-400-2006-015.* . Sacramento, CA, USA: California Energy Commission.

CEDD. (2015). *The CEDD 2010 LiDAR Survey (private communication).* Hong Kong: Civil Engineering and Development Department.

Chen, J., Kira, Z., & Cho, Y. K. (2019). Deep learning approach to point cloud scene understanding for automated scan to 3D reconstruction. *Journal of Computing in Civil Engineering, 33*(4), 04019027. doi:10.1061/(ASCE)CP.1943-5487.0000842

Chen, K., Lu, W., Peng, Y., Rowlinson, S., & Huang, G. Q. (2015). Bridging BIM and building: From a literature review to an integrated conceptual framework.

International journal of project management, 33(6), 1405-1416. doi:10.1016/j.ijproman.2015.03.006

Chen, K., Lu, W., Xue, F., Tang, P., & Li, L. H. (2018). Automatic building information model reconstruction in high-density urban areas: Augmenting multi-source data with architectural knowledge. *Automation in Construction, 93*, 22-34. doi:10.1016/j.autcon.2018.05.009

Eastman, C., Teicholz, P., Sacks, R., & Liston, K. (2011). *BIM handbook: A guide to building information modeling for owners, managers, designers, engineers and contractors* (2nd ed.). Hoboken, USA: John Wiley & Sons.

Ellenberg, A., Kontsos, A., Moon, F., & Bartoli, I. (2016). Bridge related damage quantification using unmanned aerial vehicle imagery. *Structural Control and Health Monitoring, 23*(9), 1168-1179. doi:10.1002/stc.1831

Grieves, M., & Vickers, J. (2017). Digital twin: Mitigating unpredictable, undesirable emergent behavior in complex systems. In F.-J. Kahlen, S. Flumerfelt, & A. Alves, *Transdisciplinary Perspectives on Complex Systems: New Findings and Approaches* (pp. 85-113). Springer.

Hamledari, H., McCabe, B., & Davari, S. (2017). Automated computer vision-based detection of components of under-construction indoor partitions. *Automation in Construction, 74*, 78-94. doi:https://doi.org/10.1016/j.autcon.2016.11.009

Hidaka, N., Michikawa, T., Motamedi, A., Yabuki, N., & Fukuda, T. (2018). Polygonization of point clouds of repetitive components in civil infrastructure based on geometric similarities. *Automation in Construction, 86*, 99-117. doi:10.1016/j.autcon.2017.10.014

Hsu, H. C., Chang, S., Chen, C. C., & Wu, I. C. (2020). Knowledge-based system for resolving design clashes in building information models. *Automation in Construction, 110*, 103001. doi:10.1016/j.autcon.2019.103001

Hsua, H. C., & Wua, I. C. (2019). Employing Simulated Annealing Algorithms to Automatically Resolve MEP Clashes in Building Information Modeling Models. *Proceedings of the International Symposium on Automation and Robotics in Construction (Vol. 36)* (pp. 788-795). Waterloo: IAARC. doi:10.22260/ISARC2019/0106

Jardim-Goncalves, R., Sarraipa, J., Agostinho, C., & Panetto, H. (2011). Knowledge framework for intelligent manufacturing systems. *Journal of Intelligent Manufacturing, 22*(5), 725-735. doi:10.1007/s10845-009-0332-4

Javanmardi, M., Gu, Y., Javanmardi, E., Hsu, L. T., & Kamijo, S. (2015). 3D building map reconstruction in dense urban areas by integrating airborne laser point cloud with 2D

boundary map. *Proceedings of the 2015 IEEE International Conference on Vehicular Electronics and Safety* (pp. 126-131). IEEE. doi:10.1109/ICVES.2015.7396906

Jung, J., Hong, S., Jeong, S., Kim, S., Cho, H., Hong, S., & Heo, J. (2014). Productive modeling for development of as-built BIM of existing indoor structures. *Automation in Construction, 42*, 68-77. doi:10.1016/j.autcon.2014.02.021

Kim, C., Son, H., & Kim, C. (2013). Automated construction progress measurement using a 4D building information model and 3D data. *Automation in Construction, 31*, 75-82. doi:10.1016/j.autcon.2012.11.041

Koppula, H. S., Anand, A., Joachims, T., & Saxena, A. (2011). Semantic labeling of 3d point clouds for indoor scenes. *Advances in neural information processing systems*, (pp. 244-252). doi:http://papers.nips.cc/paper/4226-semantic-labeling-of-3d-point-clouds-for-indoor-scenes.pdf

Lacasta, J., Nogueras-Iso, J., Falquet, G., Teller, J., & Zarazaga-Soria, F. J. (2013). Design and evaluation of a semantic enrichment process for bibliographic databases. *Data & Knowledge Engineering, 88*(C), 94-107. doi:10.1016/j.datak.2013.10.001

Levinson, R., Chen, S., Berdahl, P., Rosado, P., & Medina, L. A. (2014). Reflectometer measurement of roofing aggregate albedo. *Solar Energy, 100*, 159-171. doi:10.1016/j.solener.2013.11.006

Liao, Y., Lezoche, M., Panetto, H., & Boudjlida, N. (2016). Semantic annotations for semantic interoperability in a product lifecycle management context. *International Journal of Production Research, 54*(18), 5534-5553. doi:10.1080/00207543.2016.1165875

Lin, H., Gao, J., Zhou, Y., Lu, G., Ye, M., Zhang, C., . . . Yang, R. (2013). Semantic decomposition and reconstruction of residential scenes from LiDAR data. *ACM Transactions on Graphics, 32*(4), 1-10. doi:10.1145/2461912.2461969

Liu, J., & Wu, Z. (2016). Rule-based generation of ancient Chinese architecture from the Song Dynasty. *Journal on Computing and Cultural Heritage, 9*(2), Article 7. doi:10.1145/2835495

Lu, W., Lai, C. C., & Tse, T. (2019). *BIM and Big Data for Construction Cost Management.* Abingdon, Oxon: Routledge.

Mehta, M., Johnson, J., & Rocafort, J. (1999). *Architectural acoustics: Principles and design.* Englewood Cliffs, NJ United States: Prentice Hall.

Nguyen, C. H., & Choi, Y. (2018). Comparison of point cloud data and 3D CAD data for on-site dimensional inspection of industrial plant piping systems. *Automation in Construction, 91*, 44-52. doi:10.1016/j.autcon.2018.03.008

NIBS. (2015). *Standard National BIM Standard - United States Version 3.* National Institute of Building Sciences. Retrieved September 24, 2019, from https://bit.ly/33gTWZ4

NIC. (2017). *Data for the Public Good.* London: National Infrastructure Commission, UK. Retrieved from https://www.nic.org.uk/publications/data-public-good/

Pătrăucean, V., Armeni, I., Nahangi, M., Yeung, J., Brilakis, I., & Haas, C. (2015). State of research in automatic as-built modelling. *Advanced Engineering Informatics, 29*(2), 162-171. doi:10.1016/j.aei.2015.01.001

Pierdicca, R., Paolanti, M., Matrone, F., Martini, M., Morbidoni, C., Malinverni, E. S., . . . Lingua, A. M. (2020). Point cloud semantic segmentation using a deep learning framework for cultural heritage. *Remote Sensing, 12*(6), 1005. doi:10.3390/rs12061005

Rose, L. S., Akbari, H., & Taha, H. (2003). *Characterizing the fabric of the urban environment: a case study of Greater Houston, Texas.* Berkeley, CA, USA: Lawrence Berkeley National Laboratory.

Sacks, R., Ma, L., Yosef, R., Borrmann, A., Daum, S., & Kattel, U. (2017). Semantic enrichment for building information modeling: Procedure for compiling inference rules and operators for complex geometry. *Journal of Computing in Civil Engineering, 31*(6), 04017062. doi:10.1061/(asce)cp.1943-5487.0000705

Santamouris, M. (2014). Cooling the cities–a review of reflective and green roof mitigation technologies to fight heat island and improve comfort in urban environments. *Solar energy, 103*, 682-703. doi:10.1016/j.solener.2012.07.003

Schnabel, R., Wahl, R., & Klein, R. (2007). Efficient RANSAC for point-cloud shape detection. *Computer GraphicsF forum, 26*(2), 214-226. doi:10.1111/j.1467-8659.2007.01016.x

Shamir, A. (2008). A survey on mesh segmentation techniques. *Computer Graphics Forum, 27*(6), 1539-1556. doi:10.1111/j.1467-8659.2007.01103.x

Stewart, I. D., Oke, T. R., & Krayenhoff, E. S. (2014). Evaluation of the 'local climate zone'scheme using temperature observations and model simulations. *International journal of climatology, 24*(4), 1062-1080. doi:10.1002/joc.3746

Tan, T., Chen, K., Lu, W., & Xue, F. (2019). Semantic enrichment for rooftop modeling using aerial LiDAR reflectance. *Proceedings of the 2019 IEEE International Conference on Signal Processing, Communications and Computing.* IEEE. doi:10.1109/ICSPCC46631.2019.8960769

Valero, E., Adán, A., & Cerrada, C. (2012). Automatic method for building indoor boundary models from dense point clouds collected by laser scanners. *Sensors, 12*(12), 16099-16115. doi:10.3390/s121216099

Wang, J., Wu, Q., Remil, O., Yi, C., Guo, Y., & Wei, M. (2018). Modeling indoor scenes with repetitions from 3D raw point data. *Computer-Aided Design, 94*, 1-15. doi:10.1016/j.cad.2017.09.001

Wang, Q., & Kim, M. K. (2019). Applications of 3D point cloud data in the construction industry: A fifteen-year review from 2004 to 2018. *Advanced Engineering Informatics, 39*, 306-319. doi:10.1016/j.aei.2019.02.007

Xiong, X., Adan, A., Akinci, B., & Huber, D. (2013). Automatic creation of semantically rich 3D building models from laser scanner data. *Automation in Construction, 31*, 325-337. doi:10.1016/j.autcon.2012.10.006

Xu, J., Chen, K., Zetkulic, A. E., Xue, F., Lu, W., & Niu, Y. (2020). Pervasive sensing technologies for facility management: A critical review. *Facilities, 38*(1/2), 161-180. doi:10.1108/F-02-2019-0024

Xue, F., & Lu, W. (2020a). A semantic differential transaction approach to minimizing information redundancy for BIM and blockchain integration. *Automation in Construction, 118*, 103270. doi:10.1016/j.autcon.2020.103270

Xue, F., Lu, W., & Chen, K. (2018). Automatic Generation of Semantically Rich As-Built Building Information Models Using 2D Images: A Derivative-Free Optimization Approach. *Computer-Aided Civil and Infrastructure Engineering, 33*(11), 926-942. doi:10.1111/mice.12378

Xue, F., Lu, W., Chen, K., & Webster, C. J. (2019a). BIM reconstruction from 3D point clouds: A semantic registration approach based on multimodal optimization and architectural design knowledge. *Advanced Engineering Informatics, 42*, 100965. doi:10.1016/j.aei.2019.100965

Xue, F., Lu, W., Chen, K., & Zetkulic, A. (2019b). From semantic segmentation to semantic registration: Derivative-free optimization-based approach for automatic generation of semantically rich as-built Building Information Models from 3D point clouds. *Journal of Computing in Civil Engineering, 33*(4), 04019024. doi:10.1061/(ASCE)CP.1943-5487.0000839

Xue, F., Lu, W., Chen, Z., & Webster, C. J. (2020b). From LiDAR point cloud towards digital twin city: Clustering city objects based on Gestalt principles. *ISPRS Journal of Photogrammetry and Remote Sensing, 167*, 418-431. doi:10.1016/j.isprsjprs.2020.07.020

Xue, F., Lu, W., Tan, T., & Chen, K. (2019c). Semantic enrichment of city information models with LiDAR-based rooftop albedo. *Sustainable Buildings and Structures: Building a Sustainable Tomorrow: Proceedings of the 2nd International Conference in Sutainable Buildings and Structures* (p. 207). CRC Press. doi:10.1201/9781003000716-27

Xue, F., Wu, L., & Lu, W. (2021). Semantic enrichment of Building and City Information Models: a ten-year review. *Advanced Engineering Informatics*, in press.

Yang, B., Liu, B., Zhu, D., Zhang, B., Wang, Z., & Lei, K. (2020). Semiautomatic Structural BIM-Model Generation Methodology Using CAD Construction Drawings. *Journal of Computing in Civil Engineering, 34*(3), 04020006. doi:10.1061/(ASCE)CP.1943-5487.0000885